Multi-voxel algorithm for quantitative bi-exponential MRI T_1 estimation

Bladt, P.; Van Steenkiste, G.; Ramos-Llordén, G.; Den Dekker, A. J.; Sijbers, J.

DOI
10.1117/12.2216831

Publication date
2016

Document Version
Final published version

Published in
Proceedings of SPIE

Multi-voxel Algorithm for Quantitative Bi-exponential MRI T_1 Estimation

P. Bladt[1], G. Van Steenkiste[1], G. Ramos-Llordén[1], A.J. den Dekker[1,2], J. Sijbers[1]

[1] iMinds Vision Lab, University of Antwerp, Belgium.
[2] Delft Center for Systems and Control, Delft University of Technology, The Netherlands.

ABSTRACT

Quantification of the spin-lattice relaxation time, T_1, of tissues is important for characterization of tissues in clinical magnetic resonance imaging (MRI). In T_1 mapping, T_1 values are estimated from a set of T_1-weighted MRI images. Due to the limited spatial resolution of the T_1-weighted images, one voxel might consist of two tissues, causing partial volume effects (PVE). In conventional mono-exponential T_1 estimation, these PVE result in systematic errors in the T_1 map. To account for PVE, single-voxel bi-exponential estimators have been suggested. Unfortunately, in general, they suffer from low accuracy and precision. In this work, we propose a joint multi-voxel bi-exponential T_1 estimator (JMBE) and compare its performance to a single-voxel bi-exponential T_1 estimator (SBE). Results show that, in contrast to the SBE, and for clinically achievable single-voxel SNRs, the JMBE is accurate and efficient if four or more neighboring voxels are used in the joint estimation framework. This illustrates that, for clinically realistic SNRs, accurate results for quantitative bi-exponential T_1 estimation are only achievable if information of neighboring voxels is incorporated.

Keywords: Quantitative MRI, Partial volume effects, T_1 relaxometry, Maximum likelihood estimation

1 INTRODUCTION

One of the key assets of magnetic resonance imaging (MRI) as a diagnostic tool is the non-invasive provision of unique anatomical information due to a high contrast between different soft tissues in the human body. The intensities of the voxels in MR images depend on multiple variables, including the imaging sequence and the acquisition parameters. Therefore, MR images only provide qualitative information in the form of contrast between different types of tissues. Quantitative MRI methods are designed to estimate MRI parameters that provide quantitative information on tissue structure. Compared to qualitative MR images, quantitative information has more clinical significance, is easier to evaluate, allows for comparison between measurements from different scanners and enables longitudinal follow-up of patients.

The spin-lattice relaxation time, T_1, is one of the MRI parameters reflecting the local tissue environment. Quantitative T_1 mapping is a technique in which a T_1 value is estimated for each voxel in the image, using a set of T_1-weighted MR images. In conventional quantitative T_1 mapping, it is tacitly assumed that there is only one type of tissue in each voxel of the T_1-weighted images. Then, the relaxation process is described by one T_1 value. This justifies the use of voxel-wise mono-exponential models to describe the evolution of the signal intensities of T_1-weighted images acquired at different points in time. However, at borders between tissues it is possible that there are two (or more) tissue types present in a voxel, referred to as the partial volume effect (PVE). This implies that the relaxation process is described by more than one T_1 value. Quantitative multi-exponential T_1 mapping refers to methods that can detect and estimate multiple relaxation parameters in a single voxel avoiding PVEs in order to enhance the quality of the T_1 map.

If there are two tissue types present in a voxel, a bi-exponential model is needed to describe the longitudinal relaxation of the magnetization. For single-voxel multi-exponential analysis of relaxation decays, evidence is given that there is large uncertainty of the fitted parameters and that different combinations of parameters can fit the data equally well when noise is present.[1,2] Therefore, it is expected that single-voxel bi-exponential estimators for quantitative bi-exponential T_1 estimation will be inaccurate at low signal-to-noise ratios (SNRs). Several authors have proposed methods to improve the fitting of multi-exponential signals, including the use of prior information[3,4] and spatial averaging.[5–7] Huang et al.[8] presented a fitting procedure based on a multi-voxel algorithm. They estimate T_2 (spin-spin relaxation) values in the presence of PVEs based on the assumption that there are two homogeneous tissues within a region of interest (ROI) of a few neighbouring voxels. Both T_2 values are estimated jointly for all voxels within this ROI, justified by the homogeneity

Further author information: piet.bladt@uantwerpen.be

Medical Imaging 2016: Image Processing, edited by Martin A. Styner, Elsa D. Angelini, Proc. of SPIE Vol. 9784, 978402 · © 2016 SPIE
CCC code: 1605-7422/16/$18 · doi: 10.1117/12.2216831

of the tissues. This multi-voxel algorithm increases the effective SNR, thereby increasing the accuracy and precision of the estimator.

In this study, a joint multi-voxel bi-exponential estimator (JMBE) for quantitative bi-exponential T_1 estimation in the human brain is presented based on the idea introduced by Huang et al.[8] In order to create the JMBE, it is assumed that within a small region of interest of K voxels in the human brain, located at the border between two tissues, a maximum of two homogeneous tissues is present. Furthermore, the model needed to describe the longitudinal signal poses extra challenges in the implementation of the estimator compared to the simpler model for T_2 decay. Additionaly, the fact that magnitude data is Rician distributed should be accounted for in the estimation framework. These challenges are explored in this work.

2 METHODS

For quantitative bi-exponential T_1 estimation, two key pilars are needed: a robust model describing bi-exponential T_1 relaxation and a parameter estimation technique. The model for bi-exponential T_1 relaxation is built up starting from a robust model for mono-exponential T_1 relaxation. Maximum likelihood estimation is chosen as estimation technique. Both the JMBE and the SBE are constructed based on these two pilars.

2.1 Mono-exponential model

Throughout this work, it is assumed that the T_1-weighted images are acquired with the inversion-recovery gradient-echo (IR-GE) sequence, the gold standard for T_1-weighted imaging.[9,10] The magnitude signal in a voxel, containing one tissue type, of an image acquired with the IR-GE sequence is described by

$$S(\mathrm{TI}) = M_0 \left| \frac{1 - (1 - \cos(\theta_1)) \exp\left(-\frac{\mathrm{TI}}{T_1}\right) - \cos(\theta_1) \exp\left(-\frac{\mathrm{TR}}{T_1}\right)}{1 - \cos(\theta_1)\cos(\theta_2) \exp\left(-\frac{\mathrm{TR}}{T_1}\right)} \right|, \tag{1}$$

where M_0 is the equilibrium magnetization, θ_1 the angle of the inversion pulse, θ_2 the angle of the pulse that brings the longitudinal magnetization in the transverse plane for measurement, TR the repetition time and TI (inversion time) the time between the inversion pulse and the pulse bringing the magnetization in the transverse plane. By changing the TI, multiple images with different T_1-weighting can be acquired. Subsequently, mono-exponential T_1 mapping can be performed by fitting a model, related to Eq.(1), to each voxel in the set of T_1-weighted images. Assuming ideal imaging conditions ($\theta_1 = 180°$, $\theta_2 = 90°$ and TR $\gg T_1$), Eq.(1) simplifies to a frequently used model:[11]

$$f_i(\boldsymbol{\theta}) = M_0 \left| 1 - 2 \exp\left(-\frac{\mathrm{TI}_i}{T_1}\right) \right|, \tag{2}$$

with parameter vector $\boldsymbol{\theta} = \{M_0, T_1\}$. However, these assumptions are often invalid. First, a very long TR is impractical in a clinical setting as this would result in a very long total acquisition time. Furthermore, the flip angles θ_1 and θ_2 often slightly deviate from the ideal values due to inhomogeneities in the RF pulses.[11] Therefore, using Eq.(2) as model for mono-exponential T_1 mapping might result in systematic errors. A more robust model is presented by Barral et al. in:[11]

$$f_i(\boldsymbol{\theta}) \equiv f_i(a, b, T_1) = \left| a + b \exp\left(-\frac{\mathrm{TI}_i}{T_1}\right) \right|, \tag{3}$$

with parameters a and b of $\boldsymbol{\theta} = \{a, b, T_1\}$ defined as:

$$a = M_0 \frac{1 - \cos(\theta_1) \exp\left(-\frac{\mathrm{TR}}{T_1}\right)}{1 - \cos(\theta_1)\cos(\theta_2) \exp\left(-\frac{\mathrm{TR}}{T_1}\right)}, \tag{4}$$

and

$$b = -M_0 \frac{1 - \cos(\theta_1)}{1 - \cos(\theta_1)\cos(\theta_2) \exp\left(-\frac{\mathrm{TR}}{T_1}\right)}, \tag{5}$$

respectively. Up to this point, it is assumed that a voxel contains one tissue type. The model in Eq.(3) serves as a starting point for the bi-exponential model described in the next subsection.

2.2 Bi-exponential Model

Consider a voxel that contains two tissues, denoted by x and y, with spin-lattice relaxation times $\{T_{1,x}, T_{1,y}\}$ and relative volumes $\{V_x, V_y\}$, with $V_x + V_y = 1$. It can be assumed that the longitudinal relaxation of the spin systems of both tissues do not influence one another.[12,13] The resulting (noise-free) magnitude signal from an IR-GE sequence, with an inversion time TI_i, is then given by:

$$S(\text{TI}_i) = \left| V_x \left[a_x + b_x \exp\left(-\frac{\text{TI}_i}{T_{1,x}} \right) \right] + V_y \left[a_y + b_y \exp\left(-\frac{\text{TI}_i}{T_{1,y}} \right) \right] \right|, \tag{6}$$

with a_x and a_y described by Eq.(4) and b_x and b_y described by Eq.(5). By redefining the linear parameters in Eq.(6), a single-voxel bi-exponential model is given by

$$f_i(\boldsymbol{\theta}) = \left| a + b \exp\left(-\frac{\text{TI}_i}{T_{1,x}} \right) + c \exp\left(-\frac{\text{TI}_i}{T_{1,y}} \right) \right|, \tag{7}$$

with $\boldsymbol{\theta} = \{a, b, c, T_{1,x}, T_{1,y}\}$ and linear parameters $a = V_x a_x + V_y a_y$, $b = V_x b_x$ and $c = V_y b_y$.

2.3 Maximum Likelihood Estimation

The second pilar needed to construct the JMBE and the SBE is a suitable parameter estimation framework. An important feature of maximum likelihood (ML) estimation is the fact that the data distribution is incorporated in the ML estimator, in contrast to conventional (weighted) least squares estimators.

Magnitude MR data are Rician distributed with a probability density function (PDF) given by:[14–16]

$$p_M(M_i|\boldsymbol{\theta}, \sigma) = \frac{M_i}{\sigma^2} \exp\left(-\frac{M_i^2 + f_i^2(\boldsymbol{\theta})}{2\sigma^2} \right) I_0\left(\frac{f_i(\boldsymbol{\theta}) M_i}{\sigma^2} \right), \tag{8}$$

with $I_0(.)$ the zeroth order modified Bessel function of the first kind, M_i a voxel value of the magnitude image at inversion time TI_i, σ the standard deviation of the Gaussian noise in the real and imaginary images and $f_i(\boldsymbol{\theta})$ the model, a function of the $\boldsymbol{\theta}$, describing the magnitude data at inversion time TI_i.

Consider a set of N independent magnitude MR data points $\{M_i\}_{i=1}^N$ measured at N inversion time points TI_i. The joint probability density function $p_M(\{M_i\}|\boldsymbol{\theta}, \sigma)$ of these data points is the product of the marginal PDFs of the individual data points, assuming independence between acquisitions:

$$p_M(\{M_i\}|\boldsymbol{\theta}, \sigma) = \prod_{i=1}^{N} p_M(M_i|\boldsymbol{\theta}, \sigma). \tag{9}$$

The joint PDF is a function of the data for a given value of the parameters. The ML estimator is derived from this joint PDF as follows.[17] First, the available data points are substituted for the corresponding independent variables in the joint PDF. Since these data points are numbers, the resulting expression depends only on the elements of the parameter vector $\boldsymbol{\theta}$. These elements, which are the hypothetical true parameters, are now considered to be variables. The resulting function is called the likelihood function, which is denoted as $L(\boldsymbol{\theta}|\{M_i\})$ It follows from Eqs. (8) and (9) that the likelihood function is given by:[18]

$$L(\boldsymbol{\theta}|\{M_i\}) = \frac{1}{\sigma^{2N}} \exp\left(-\sum_{i=1}^{N} \frac{M_i^2 + f_i(\boldsymbol{\theta})^2}{2\sigma^2} \right) \prod_{i=1}^{N} M_i I_0\left(\frac{f_i(\boldsymbol{\theta}) M_i}{\sigma^2} \right). \tag{10}$$

The ML estimator $\hat{\boldsymbol{\theta}}_{ML}$ is now defined as the value of $\boldsymbol{\theta}$ that maximizes the likelihood function with respect to $\boldsymbol{\theta}$:

$$\hat{\boldsymbol{\theta}}_{ML} = \arg\max_{\boldsymbol{\theta}} (L(\boldsymbol{\theta}|\{M_i\})). \tag{11}$$

2.4 Joint Multi-voxel Bi-exponential Estimator

The JMBE is constructed with the single-voxel bi-exponential model described in Eq.(7) and the ML estimation framework described in the previous subsection.

Consider K voxels in a chosen ROI that contains two homogeneous tissues with global spin-lattice relaxation times $\bar{T}_{1,x}$ and $\bar{T}_{1,y}$. The likelihood function of N observed magnitude data points in each of the K voxels, assuming independence between all data points (between acquisitions on the one hand and between voxels on the other hand), is given by:

$$L(\boldsymbol{\theta}|\{M_{i,k}\}) = \prod_{k=1}^{K}\prod_{i=1}^{N} p_M(M_{i,k}|f_{i,k}(\boldsymbol{\theta}_k),\sigma) \tag{12}$$

$$= \frac{1}{\sigma^{2NK}} \exp\left(-\sum_{k=1}^{K}\sum_{i=1}^{N}\frac{M_{i,k}^2 + f_{i,k}(\boldsymbol{\theta}_k)^2}{2\sigma^2}\right) \prod_{k=1}^{K}\prod_{i=1}^{N} M_{i,k} I_0\left(\frac{f_{i,k}(\boldsymbol{\theta}_k)M_{i,k}}{\sigma^2}\right), \tag{13}$$

with $\boldsymbol{\theta} = \{a_1, ..., a_K, b_1, ..., b_K, c_1, ..., c_K, \bar{T}_{1,x}, \bar{T}_{1,y}\}$, $\boldsymbol{\theta}_k = \{a_k, b_k, c_k, \bar{T}_{1,x}, \bar{T}_{1,y}\}$, $M_{i,k}$ the magnitude signal of voxel k at time i and $f_{i,k}(\boldsymbol{\theta}_k)$ the single-voxel bi-exponential model in Eq.(7):

$$f_{i,k}(\boldsymbol{\theta}_k) = \left| a_k + b_k \exp\left(-\frac{\mathrm{TI}_i}{\bar{T}_{1,x}}\right) + c_k \exp\left(-\frac{\mathrm{TI}_i}{\bar{T}_{1,y}}\right)\right|. \tag{14}$$

The JMBE searches for the $\boldsymbol{\theta}$, consisting of $3K$ linear and 2 nonlinear parameters, that maximizes the likelihood function defined by Eq.(13). Since the logarithm is a monotonically increasing function, maximizing the likelihood function is equivalent to minimizing the negative logarithm of the likelihood function, which is computationally less demanding:[19]

$$\hat{\boldsymbol{\theta}}_{ML} = \arg\min_{\boldsymbol{\theta}}\left(\sum_{k=1}^{K}\sum_{i=1}^{N}\left[\frac{f_{i,k}(\boldsymbol{\theta}_k)^2}{2\sigma^2} - \ln I_0\left(\frac{f_{i,k}(\boldsymbol{\theta}_k)M_{i,k}}{\sigma^2}\right)\right]\right). \tag{15}$$

In human tissue, perfect homogeneity is not expected and the T_1 value of a tissue type within the ROI might vary slightly. Therefore, the global spin-lattice relaxation time of a tissue type x in a ROI of K voxels is given by the weighted average:

$$\bar{T}_{1,x} = \frac{\sum_{k=1}^{K} V_{1,k} T_{1,x,k}}{\sum_{k=1}^{K} V_{1,k}}, \tag{16}$$

with $V_{1,k}$ the relative volume of the tissue type x in voxel k and $T_{1,x,k}$ the spin-lattice relaxation time of tissue type x in voxel k.

The SBE, which serves as an initial comparison for the JMBE, can be seen as a special case of the JMBE. Indeed, the JMBE transforms to the SBE when $K = 1$, i.e., the ROI consists of one voxel. Furthermore, the global spin-lattice relaxation times, $\bar{T}_1$, reduce to the voxel spin-lattice relaxation times, T_1. The parameter vector $\boldsymbol{\theta}$ consists of 3 linear and 2 nonlinear parameters: $\boldsymbol{\theta} = \{a, b, c, T_{1,x}, T_{1,y}\}$.

The JMBE and SBE are constructed in Matlab (The Mathworks, Natick, MA, United States). The minimization of the negative logarithm of the likelihood function is performed using unconstrained nonlinear optimization Matlab functions. More specifically, the Matlab function *fminunc* is used as it attempts to find a minimum of a nonlinear multivariable function starting at an initial estimate. Within the function *fminunc*, the *trust-region* algorithm is chosen to perform the optimization. This algorithm requires the gradient of the function with respect to the elements in $\boldsymbol{\theta}$, which drastically speeds up the search for the minimum. The initial estimate of $\boldsymbol{\theta}$ is obtained in two steps. First, the polarity of the magnitude data is restored by applying a sign-shifting function.[11] Then, a starting point is found by means of a nonlinear least squares fit using the variable projection algorithm.[20]

2.5 Cramér-Rao Lower Bound

The bias of an estimator $\hat{\boldsymbol{\theta}}$ is defined as

$$\boldsymbol{b}(\hat{\boldsymbol{\theta}}) = E[\hat{\boldsymbol{\theta}}] - \boldsymbol{\theta}, \tag{17}$$

with $E[.]$ the expectation operator and $\boldsymbol{\theta}$ the true (unknown) parameter vector. If $\boldsymbol{b}(\hat{\boldsymbol{\theta}}) = \mathbf{0}$, the estimator is unbiased. The CRLB is a lower bound on the variance of any unbiased estimator $\hat{\boldsymbol{\theta}}$ of the parameter vector $\boldsymbol{\theta}$:[21]

$$\text{cov}(\hat{\boldsymbol{\theta}}) \geq I(\boldsymbol{\theta})^{-1}, \tag{18}$$

with $\text{cov}(\hat{\boldsymbol{\theta}})$ the covariance matrix of $\hat{\boldsymbol{\theta}}$, $I(\boldsymbol{\theta})$ the Fisher information matrix and the symbol $\geq$ implying that the matrix difference $\text{cov}(\hat{\boldsymbol{\theta}}) - I(\boldsymbol{\theta})^{-1}$ is a positive semidefinite matrix. In other words, the variances of the elements of $\hat{\boldsymbol{\theta}}$ (i.e., the diagonal elements of $\text{cov}(\hat{\boldsymbol{\theta}})$) are always higher than or equal to the corresponding diagonal elements of the inverse of the Fisher information matrix. The Fisher information matrix is defined as

$$I(\boldsymbol{\theta}) = E\left[\left(\frac{\partial \ln p(\boldsymbol{y}|\boldsymbol{\theta})}{\partial \boldsymbol{\theta}}\right)\left(\frac{\partial \ln p(\boldsymbol{y}|\boldsymbol{\theta})}{\partial \boldsymbol{\theta}}\right)^{T}\right], \tag{19}$$

with $p(\boldsymbol{y}|\boldsymbol{\theta})$ the PDF given a certain parameter vector $\boldsymbol{\theta}$. For Rician magnitude data, the PDF is given by Eq.(8). Substitution of the joint PDF, defined in Eq.(12), in Eq.(19), results in:[22]

$$I(\boldsymbol{\theta}) = \sum_{k=1}^{K}\sum_{i=1}^{N}\frac{\partial f_{i,k}}{\partial \boldsymbol{\theta}}\frac{\partial f_{i,k}}{\partial \boldsymbol{\theta}^{T}}\int_{M_{i,k}=0}^{\infty}\frac{M_{i,k}}{\sigma^2}\exp\left(-\frac{M_{i,k}^2+f_{i,k}^2}{2\sigma^2}\right)I_0\left(\frac{M_{i,k}f_{i,k}}{\sigma^2}\right)\left(\frac{M_{i,k}I_1\left(\frac{M_{i,k}f_{i,k}}{\sigma^2}\right)}{\sigma^2 I_0\left(\frac{M_{i,k}f_{i,k}}{\sigma^2}\right)}-\frac{f_{i,k}}{\sigma^2}\right)^2 dM_{i,k}. \tag{20}$$

with model $f_{i,k} \equiv f_{i,k}(\boldsymbol{\theta}_k)$. The integral in Eq.(20) can only be computed numerically.

An unbiased estimator with a variance that approaches the CRLB (i.e., an estimator with maximally achievable precision) is referred to as efficient.[23] The efficiency of an estimator is defined as the ratio of the relevant CRLB variance to the variance of the estimator.[24] The ML estimator is an asymptotically efficient estimator, i.e., it reaches the CRLB asymptotically (that is, for an increasing number of observations).[19,25]

By implementing the model given by Eq.(14) in Eq.(20), the CRLBs can be calculated and compared to the precision of the JMBE to determine its efficiency. As the SBE is a special case of the JMBE, the CRLBs needed for assessment of the efficiency of the SBE are found analogously with $K = 1$.

3 EXPERIMENTS AND RESULTS

3.1 Single-voxel Bi-exponential T_1 Estimation

It is expected that single-voxel bi-exponential T_1 estimation is inaccurate at clinically realistic SNRs, based on previous research of single-voxel multi-exponential analysis of relaxation decays.[1,2] This premise was explored with a numerical simulation experiment using the SBE.

A voxel was created containing 50% white matter ($V_w = 0.5$, $M_0 = 0.69$, $T_{1,\text{w}} = 815.5$ ms) and 50% gray matter ($V_g = 0.5$, $M_0 = 0.78$, $T_{1,g} = 1325.6$ ms). The chosen tissue spin-lattice relaxation times are realistic values for these tissues in a 3T MRI scanner.[26–31] For a fixed SNR, the bias of the estimator increases as the ratio $T_{1,x}/T_{1,y}$, with the largest spin-lattice time in the numerator, decreases.[2] Of the three major brain tissues (white matter, gray matter and CSF), the ratio $T_{1,x}/T_{1,y}$ is smallest for white matter (WM) and gray matter (GM). Therefore, the expected inaccuracy will be most prominent in the WM-GM combination, explaining their selection in this experiment. From this phantom voxel, noise-free IR-GE T_1-weighted magnitude data was simulated with fixed imaging settings shown in Table 1. The inversion times $\{\text{TI}_i\}_{i=1}^{N}$, at which the longitudinal magnetization is sampled, are predominantly in the beginning of the available time interval TR. This provides more information as the signal is often fully relaxed in the later parts of this time interval.

From the noise-free dataset, Rician distributed measurements were generated. For an SNR of 2000, 600, 400 and 50, this process was repeated 5000 times, resulting in 5000 noisy datasets per SNR. The SNR was defined as

$$\text{SNR} = \frac{\mu_s}{\sigma}, \tag{21}$$

with μ_s the mean of the signal intensity distribution of the N T_1-weighted magnitude images and σ the standard deviation of the Gaussian noise in the original real and imaginary images.

TR	10 s
θ_1	180°
θ_2	90°
N	12
$\{\text{TI}_i\}_{i=1}^N$	50, 81, 131, 211, 342, 553, 895, 1447, 2340, 3785, 6121 and 9900 ms

Table 1: Imaging settings for single-voxel bi-exponential simulation experiment.

From the $n = 5000$ datasets for each SNR, n estimates $\hat{\boldsymbol{\theta}}^{(1)}, \ldots, \hat{\boldsymbol{\theta}}^{(n)}$ of the underlying parameter vector $\boldsymbol{\theta}$ were obtained with the SBE. The distribution of the $T_{1,w}$ and $T_{1,g}$ estimates for the different SNRs is shown in Fig.1. As the SNR decreases, the distributions start to deviate from a normal distribution. For an SNR of 50, the estimator fails completely. In order to quantify the accuracy of the estimator, the bias of the estimator was estimated from the sample $\{\hat{\boldsymbol{\theta}}^{(1)}, \ldots, \hat{\boldsymbol{\theta}}^{(n)}\}$ for each of the different SNRs. An estimator of the bias of the m^{th} element $\hat{\theta}_m$ of $\hat{\boldsymbol{\theta}}$ is provided by

$$\hat{b}(\hat{\theta}_m) = \langle \hat{\theta}_m \rangle - \theta_m, \tag{22}$$

with $\langle \hat{\theta}_m \rangle = \frac{1}{n} \sum_{j=1}^{n} \hat{\theta}_m^{(j)}$ the sample mean. A $100 \times (1-\alpha)\%$ confidence interval (CI) for $\hat{b}(\hat{\theta}_m)$ is then given by:[32]

$$\left[\hat{b}(\hat{\theta}_m) - t_{\alpha/2,n-1} \frac{s_m}{\sqrt{n}}, \hat{b}(\hat{\theta}_m) + t_{\alpha/2,n-1} \frac{s_m}{\sqrt{n}} \right], \tag{23}$$

with $t_{\alpha/2,n-1}$ the $100 \times (1-\alpha/2)\%$-percentile of a t-distributed random variable with $n-1$ degrees of freedom and s_m the sample standard deviation defined by

$$s_m = \sqrt{\frac{1}{n-1} \sum_{i=1}^{n} (\hat{\theta}_m^{(i)} - \langle \hat{\theta}_m \rangle)^2}. \tag{24}$$

If the $100 \times (1-\alpha)\%$ CI, defined in Eq.(23), does not contain the value zero, the null hypothesis that the estimator $\hat{\theta}_m$ is unbiased is rejected with a significance level of α.

In Table 2, the bias estimates for the different SNRs are given for the relaxation parameters. For an SNR of 600, the bias for the T_1 estimation of gray matter is already significant. Little information on typical SNRs in T_1-weighted MR images was found in the literature. Based on the calculation of the SNR on a real dataset of T_1-weighted brain images (26-year old healthy male volunteer, 3T Siemens MRI scanner, IR turbo spin echo sequence, $(2 \times 2 \times 6)$ mm^3 voxels in 25 128×128 slices, TR=8040 ms, TE=18 ms, echo spacing = 8.78 ms, turbo factor = 4, bandwidth = 222 Hz/Px) and one reference,[33] it is assumed that typical T_1-weighted images acquired at 3T have an SNR between 20 and 100 depending on the voxel size. For this SNR range, Table 2 clearly shows that the SBE is unable to produce accurate estimates of $T_{1,w}$ and $T_{1,g}$ in voxels suffering from PVEs when $N = 12$ data points are used.

	White Matter		Gray Matter	
SNR	$\hat{b}(\hat{T}_{1,w})$ [ms]	CI [ms]	$\hat{b}(\hat{T}_{1,g})$ [ms]	CI [ms]
2000	-0.10	[-0.35, 0.15]	0.21	[-0.16,0.58]
600	-0.80	[-1.62,0.03]	5.3	[4.1,6.6]
400	-3.3	[-4.6,-2.0]	9.6	[7.7,11.6]
50	-105	[-113,-98]	635	[597,673]

Table 2: Estimate of the bias of the T_1 estimator for both WM (left) and GM (right), along with the 95% confidence intervals (CI). These are calculated using the results shown in Fig.1.

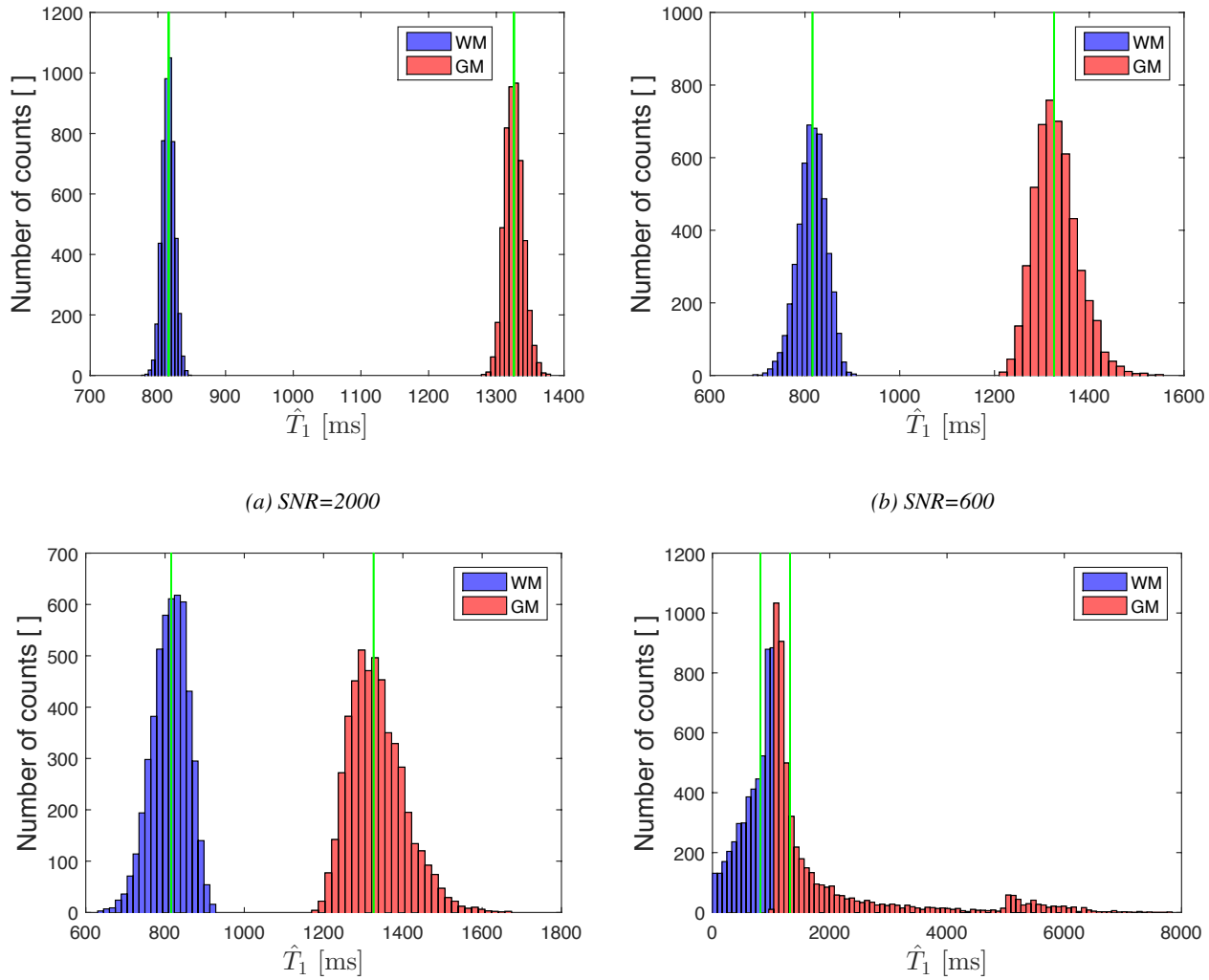

(a) SNR=2000

(b) SNR=600

(c) SNR=400

(d) SNR=50

Figure 1: $\hat{T}_1$ histograms from 2000 realizations for a voxel with a 50/50 WM/GM ratio. The green lines show the true T_1 values.

3.2 Multi-voxel Bi-exponential T_1 Estimation

In the previous subsection, it was shown that, for clinically realistic SNRs, the SBE is clearly unsuitable for bi-exponential T_1 estimation. The effective SNR can be increased by means of the JMBE as the signal of multiple voxels within the ROI is incorporated, which is expected to lead to more accurate estimation of the global spin-lattice relaxation times $\bar{T}_{1,x}$ and $\bar{T}_{1,y}$ of both tissues within the ROI. However, the ROI should be kept as small as possible to meet the demand of tissue homogeneity. If the ROI is too large, the spin-lattice relaxation time might vary substantially within a tissue, which would lead to quantification errors. With this trade-off in mind, the choice was made to define the ROI as four contiguous voxels ($K = 4$), arranged two-by-two.

There is a vast amount of possibilities for the distribution of two tissues in these four voxels. As it is not possible to study the quality of the estimator for all tissue distributions, a first evaluation of the JMBE was done using a phantom with a basic, yet probable, distribution of WM and GM (Fig.2). Two voxels contain 50% WM and 50% GM, while the other two only contain one of both tissue types. Again, WM and GM are chosen as simulation tissues since estimation inaccuracy, if present, is expected to be most prominent for this combination of brain tissues.[2] As perfect tissue homogeneity is improbable, small intra-tissue variations in voxel spin-lattice relaxation were manually introduced to make the experiment

more realistic. For WM, the $T_{1,w}$ values were 812.9 ms, 815.5 ms and 818.1 ms. For GM, 1322.1 ms, 1325.6 ms and 1329.1 ms were chosen as $T_{1,g}$ values. This resulted in global spin-lattice relaxation times $\bar{T}_{1,w} = 815.5$ ms and $\bar{T}_{1,g} = 1325.6$ ms, for WM and GM respectively.

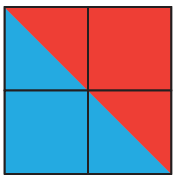

Figure 2: Schematic presentation of a distribution of WM and GM in the four-voxel phantom

The setup of this experiment is identical to the experiment performed in the previous section. From the four-voxel phantom, noise-free IR-GE T_1-weighted magnitude data was simulated with the same imaging settings as for the experiment in the previous subsection (Table 1). For multiple SNRs, Rician distributed measurements were generated 5000 times from the noise-free dataset. From the $n = 5000$ datasets for each SNR, n estimates $\hat{\boldsymbol{\theta}}^{(1)}, \ldots, \hat{\boldsymbol{\theta}}^{(n)}$ of the known true parameter vector $\boldsymbol{\theta}$ were obtained with the JMBE. The distribution of the $\bar{T}_{1,w}$ and $\bar{T}_{1,g}$ estimates for a single-voxel SNR of 200, 100, 50 and 20 are shown in Fig.3. As for the SBE experiment, the accuracy of the estimator was quantitatively judged by estimating the bias, shown in Table 3. From these results, it can be concluded that the null hypothesis that the JMBE is unbiased cannot be rejected (with a significance level of 0.05) down to an SNR of 70 for this particular distribution of tissues in the ROI when $N = 12$ magnitude data points are used. Compared to the results of the SBE, the improvement is significant.

	White Matter		Gray Matter	
SNR	$\hat{b}(\hat{\bar{T}}_{1,w})$ [ms]	CI [ms]	$\hat{b}(\hat{\bar{T}}_{1,g})$ [ms]	CI [ms]
200	0.20	[-0.14,0.54]	0.013	[-0.470,0.494]
100	0.70	[-0.17, 1.57]	0.90	[-0.38, 2.17]
70	-0.43	[-1.69,0.83]	1.5	[-0.5,3.4]
50	3.4	[1.6,5.3]	6.5	[3.7,9.3]
20	14	[9,19]	82	[71,93]

Table 3: Estimate of the bias of the $\bar{T}_1$ estimator for both WM (left) and GM (right), along with the 95% confidence intervals (CI). These are calculated using the results shown in Fig.3.

Next, the efficiency of the JMBE was estimated from the sample $\{\hat{\boldsymbol{\theta}}^{(1)}, \ldots, \hat{\boldsymbol{\theta}}^{(n)}\}$ for each SNR. As the efficiency of the estimator is defined as the ratio of the relevant CRLB variance to the variance of the estimator, an estimator of the efficiency of $\hat{\theta}_m$ is given by

$$\hat{e}(\hat{\theta}_m) = \frac{\text{CRLB}(\theta_m)}{s_m^2}, \tag{25}$$

with $\text{CRLB}(\theta_m)$ the mth element on the diagonal of the inverse of the Fisher information matrix defined in Eq.(20) and s_m the sample standard deviation defined in Eq.(24). A $100 \times (1-\alpha)\%$ CI for the efficiency is given by:[32]

$$\left[\frac{\text{CRLB}(\theta_m)}{s_m^2} \frac{\chi^2_{\alpha/2;n-1}}{n-1}, \frac{\text{CRLB}(\theta_m)}{s_m^2} \frac{\chi^2_{1-\alpha/2;n-1}}{n-1} \right], \tag{26}$$

with $\chi^2_{\alpha/2;n-1}$ the $100 \times (1-\alpha/2)\%$-percentile of a χ^2-distributed random variable with $n-1$ degrees of freedom. The null hypothesis that the estimator $\hat{\theta}_m$ is efficient is rejected (with significance level α) if the value 1 lies outside the CI. In Table 4, the effiency estimates are shown for the different SNRs. It can be concluded that the estimator, which is unbiased down to an SNR of 70, is efficient down to the same SNR for this particular distribution of WM and GM in the four-voxel ROI and assuming $N = 12$ T_1-weighted data points are used.

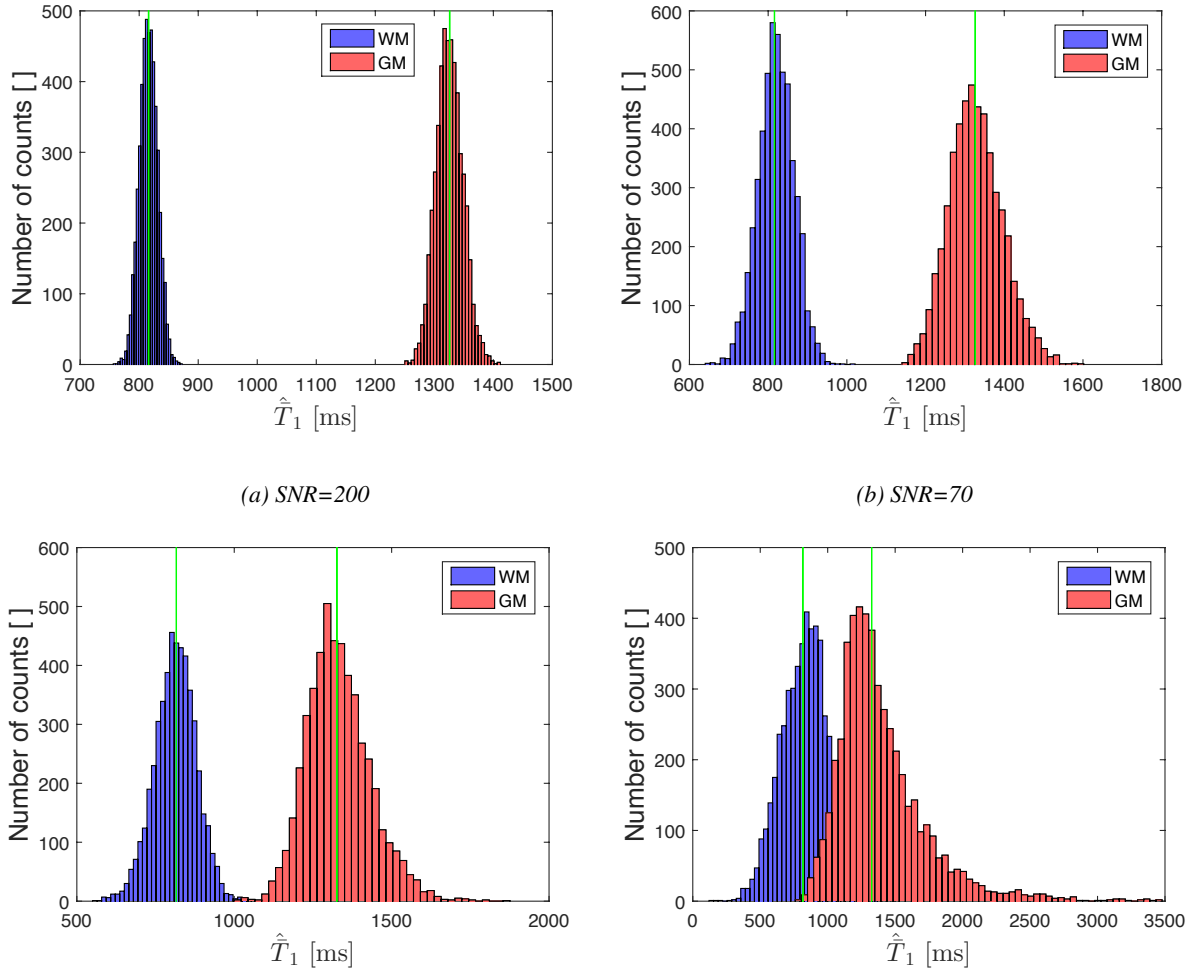

(a) SNR=200

(b) SNR=70

(c) SNR=50

(d) SNR=20

Figure 3: $\hat{\bar{T}}_1$ histograms from 5000 realizations for a four-voxel phantom containing 50% WM and 50% GM. The green lines show the true $\bar{T}_1$ values.

	White Matter		Gray Matter	
SNR	$\hat{e}(\hat{\bar{T}}_{1,w})$	CI	$\hat{e}(\hat{\bar{T}}_{1,g})$	CI
200	0.997	[0.959,1.037]	1.001	[0.962,1.041]
100	0.994	[0.965, 1.034]	0.972	[0.935, 1.011]
70	0.992	[0.953,1.031]	0.963	[0.926,1.002]
50	0.91	[0.87,0.95]	0.88	[0.84,0.92]
20	0.89	[0.86,0.92]	0.10	[0.09,0.11]

Table 4: Estimate of the efficiency of $\hat{\bar{T}}_1$ for WM (left) and GM (right) along with its 95% confidence intervals (CI). These are calculated using the results shown in Fig.3.

3.3 Criterion for Accurate and Efficient Bi-exponential T_1 Estimation

In the previous subsection, the accuracy and efficiency of the JMBE for a particular combination of tissues in four voxel was demonstrated for a clinically achievable SNR. However, as stated above, there are many possible distributions of two

tissues within a four-voxel ROI and it is impossible to validate the estimator for all these distributions. Therefore, based on the results shown in the previous subsection, a criterion was searched that provides an estimate of the minimal single-voxel SNR needed in order to produce accurate and efficient estimations of $\bar{T}_{1,x}$ and $\bar{T}_{1,y}$ with the JMBE for a particular distribution of two tissues in the ROI.

Consider the results in the previous subsection. It is clearly shown in Fig.3 that, as the SNR decreases, the precision of the estimator decreases which results in a smaller distance between the sample distributions. In Fig.3c, for an SNR of 50, the sample distributions start to overlap. Furthermore, for that SNR, each sample distribution starts to deviate from a normal distribution, most visible in the outer tail of the histogram of the GM relaxation parameter estimates. This qualitative observation was confirmed by the quantitative estimation of the bias that shows that the JMBE is biased for an SNR of 50 for that tissue distribution in the ROI. It appears that there should be a clear separation between the sample distributions for both global T_1 values. Whether there is a separation between both sample distributions, depends on the precision (i.e. standard deviation or variance) of the estimator and the absolute difference between the ground truth values of $\bar{T}_{1,w}$ and $\bar{T}_{1,g}$. As the estimator is unbiased down to an SNR of 70 in the previous experiment, the separation between both sample distributions in Fig.3b qualifies as the minimal separation for an unbiased JMBE. The relation between the sample standard deviations for $\bar{T}_{1,w}$ and $\bar{T}_{1,g}$ and the absolute difference between the ground truth values is given by:

$$|\bar{T}_{1,w} - \bar{T}_{1,g}| = 4.47(s_{\bar{T}_{1,w}} + s_{\bar{T}_{1,g}}). \tag{27}$$

Furthermore, it was shown that the JMBE is efficient if it is unbiased. Therefore, the sample standard deviations in Eq.(27) can be replaced by the respective square roots of the CRLBs. Based on these observation, a general criterion for an unbiased and efficient JMBE is provided by

$$|\bar{T}_{1,x} - \bar{T}_{1,y}| > 4.5\left(\sqrt{\text{CRLB}\left(\bar{T}_{1,x}|\boldsymbol{\theta}, N, \{\text{TI}_{i=1}^{N}\}\right)} + \sqrt{\text{CRLB}\left(\bar{T}_{1,y}|\boldsymbol{\theta}, N, \{\text{TI}_{i=1}^{N}\}\right)}\right), \tag{28}$$

with $\text{CRLB}(\bar{T}_{1,x}|\boldsymbol{\theta}, N, \{\text{TI}_{i=1}^{N}\})$ the respective element on the diagonal of the inverse of $I(\boldsymbol{\theta})$, described in Eq.(20). Note that the CRLB of $\bar{T}_{1,x}$ depends on the other parameters in $\boldsymbol{\theta}$. In other words, two ROIs with different distributions of two tissues with fixed values for $\bar{T}_{1,x}$ and $\bar{T}_{1,y}$ will have different values for the CRLBs. Furthermore, the number of T_1-weighted images N and the inversion times at which the images are acquired $\{\text{TI}_{i=1}^{N}\}$ also effect the CRLB.

With the rule of thumb defined in Eq.(28), it is possible, for any distribution of two tissues within the four-voxel ROI, to easily obtain an estimate of the minimal SNR required for the JMBE to be accurate and efficient. Instead of performing the experiment from the previous subsection for multiple distributions of tissues, this criterion allows a fast feasibility study of bi-exponential T_1 estimation with the JMBE for some expected tissue distributions.

For a certain distribution of tissues in the ROI, the sum of the square roots of the CRLBs of $\bar{T}_{1,x}$ and $\bar{T}_{1,y}$ was calculated for a range of SNRs between 5 and 100, assuming $N = 12$ T_1-weighted images acquired at the TIs shown in Table 1. This experiment was performed for multiple distributions of two tissue types in the four-voxel phantom (Fig. 4). The voxel spin-lattice relaxation times were chosen guaranteeing that $\bar{T}_{1,x}$ and $\bar{T}_{1,y}$ had the same value for the different distributions of two specific tissues. This facilitates the comparison between the different distributions. This entire process was performed for the three possible combinations of major brain tissues: WM and GM, WM and CSF, and GM and CSF. For CSF, the global spin-lattice relaxation time $\bar{T}_{1,c}$ was fixed to 4136 ms.[31]

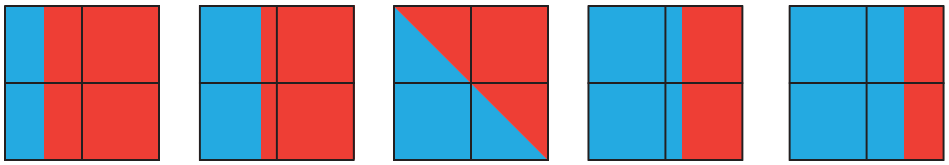

Figure 4: Schematic presentation of a four-voxel phantom containing (a) 25% WM and 75% GM, (b) 40% WM and 60% GM, (c) 50% WM and 50% GM, (d) 60% WM and 40% GM, and (e) 75% WM and 25% GM

The results are shown in Fig.5-7. For combinations of WM and GM, the minimal single-voxel SNR for an accurate and efficient JMBE lies between 60 and 90. Equivalently, for combinations of GM and CSF, and WM and CSF, the JMBE

requires a minimal SNR between 20 and 40, and 10 and 25, respectively. The results of this feasibility study are in line with the observation of Clayden et al.[2] that estimator inaccuracy is more prominent as the ratio $T_{1,x}/T_{1,y}$, with $T_{1,x} > T_{1,y}$, decreases. The combination of WM and GM determines the general SNR requirements for accurate and efficient multi-voxel bi-exponential T_1 estimation as it demands the highest single-voxel SNR. It can be concluded that, when $N = 12$ T_1-weighted images are acquired and a four-voxel ROI is chosen for the JMBE, a minimal SNR of approximately 90 is needed for accurate and efficient multi-voxel bi-exponential T_1 estimation.

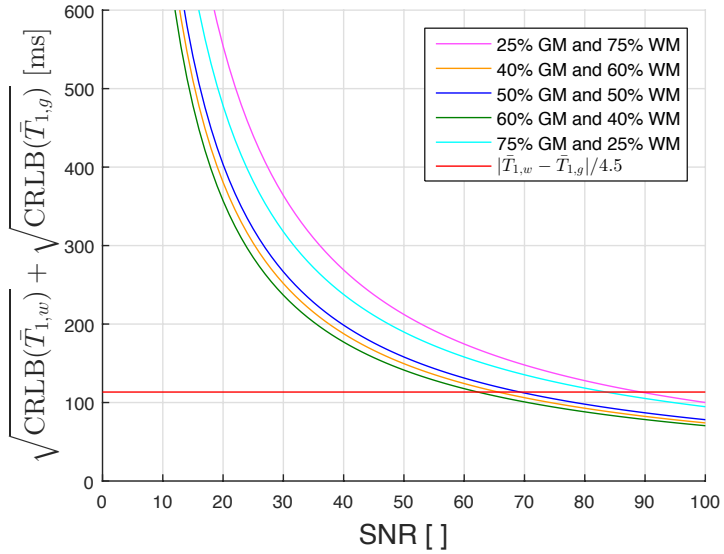

Figure 5: Feasibility study for multiple distributions of WM and GM in the ROI. The x-component of the intersection point (x, y) between each curve and the horizontal line represents the minimal single-voxel SNR needed for the JMBE to be accurate and efficient.

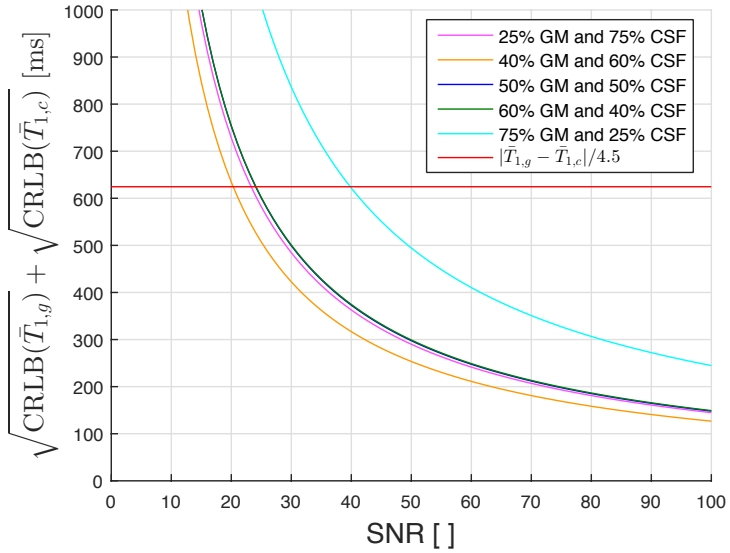

Figure 6: Feasibility study for multiple distributions of GM and CSF in the ROI. The x-component of the intersection point (x, y) between each curve and the horizontal line represents the minimal single-voxel SNR needed for the JMBE to be accurate and efficient. Note that the green and blue curve are superimposed.

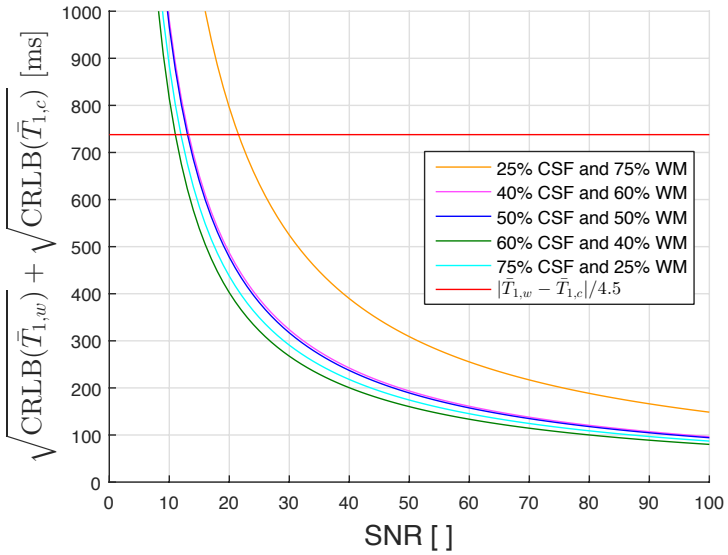

Figure 7: Feasibility study for multiple distributions of WM and CSF in the ROI. The x-component of the intersection point (x, y) between each curve and the horizontal line represents the minimal single-voxel SNR needed for the JMBE to be accurate and efficient.

4 DISCUSSION AND CONCLUSION

In this work, a joint multi-voxel bi-exponential T_1 estimator was presented to estimate the spin-lattice relaxation times of both tissues present in a ROI of neighbouring voxels containing voxels suffering from PVEs. For a ROI of four voxels, the JMBE is accurate and efficient for a minimal single-voxel SNR of 90, when 12 T_1-weighted images are obtained. This implies that, for these conditions, the JMBE is accurate and efficient around the top of the clinically achievable SNR range. This is in sharp contrast to the SBE, which was already biased for an SNR of 600, assuming 12 T_1-weighted images.

The high level of homogeneity is a vital assumption for the validity of the JMBE. If within-tissue T_1 values vary significantly on a scale comparable to the size of the ROI, it will result in quantification errors. This requires further research on in vivo data. Note, however, that when clinical data is used, JMBE quantification errors due to tissue heterogeneity will be small compared to the SBE quantification errors caused by a complete failure of the estimator at clinically realistic SNRs.

The minimal SNR required could be further lowered in two ways. A first option is the acquisition of a larger amount of T_1-weighted images. However, this has the downside of extending the total acquisition time. The second, more feasible option is enlarging the ROI to 8 neighbouring voxels, arranged $2 \times 2 \times 2$. Unfortunately, depending on the size and shape of the voxels, this might further increase the within-tissue heterogeneity. Furthermore, it would cause the addition of 12 extra linear parameters to $\boldsymbol{\theta}$.

In order to upgrade from quantitative bi-exponential T_1 estimation to quantitative bi-exponential T_1 mapping with enhancement of the quality of the T_1 map by avoiding PVEs as the final goal, two extra obstacles need to be addressed. Firstly, the relative volumes V_x and V_y of both tissues in a voxel need to be derived from the estimated linear parameters. Secondly, an algorithm is needed to distribute both relative volumes in the voxel taking into account the tissues in the neighbouring voxels. Accurate quantitative bi-exponential T_1 estimation by means of the JMBE is the first step in this three-step process towards quantitative bi-exponential T_1 mapping.

References

[1] Bretthorst, G., "How accurately can parameters from exponential models be estimated? a Bayesian view," *Concept Magn. Reson. Part A* **27**, 73–83 (2005).

[2] Clayden, N. and Hesler, B., "Multiexponential analysis of relaxation decays," *J. Magn. Reson.* **98**, 271–282 (1992).

[3] Hwang, D. and Du, Y., "Improved myelin water quantification using spatially regularized non-negative least squares algorithm," *J. Magn. Reson. Im.* **30**, 203–208 (2009).

[4] Kumar, D., Nguyen, T., Gauthier, S., and Raj, A., "Bayesian algorithm using spatial priors for multiexponential T_2 relaxometry from multiecho spin echo MRI," *Magn. Reson. Med.* **68**, 1536–1543 (2012).

[5] Anastasiou, A. and Hall, L., "Optimisation of T_2 and M_0 measurements of bi-exponential systems," *Magn. Reson. Im.* **22**, 67–80 (2004).

[6] Graham, S., Stanchev, P., and Bronskill, M., "Criteria for analysis of multicomponent tissue T_2 relaxation data," *Magn. Reson. Med.* **35**, 370–378 (1996).

[7] Bjarnason, T., McCreary, C., Dunn, J., and Mitchell, J., "Quantitative T_2 analysis: the effects of noise, regularization, and multivoxel approaches," *Magn. Reson. Med.* **63**, 212–217 (2010).

[8] Huang, C., Galons, J., Graff, C., Clarkson, E., Bilgin, A., Kalb, B., Martin, D., and Altback, M., "Correcting partial volume effects in biexponential T_2 estimation of small lesions," *Magn. Reson. Med.* **73**, 1632–1642 (2015).

[9] Drain, L., "A direct method of measuring nuclear spin-lattice relaxation times," *Proc. Phys. Soc. Section A* **62**(5), 301–306 (1949).

[10] Hahn, E., "An accurate nuclear magnetic resonance method for measuring spin-lattice relaxation times," *Phys. Rev. Lett.* **76**, 145 (1949).

[11] Barral, J., Gudmundson, E., Stikov, N., Etezadi-Amoli, M., Stoica, P., and Nishimura, D., "A robust methodology for in vivo T_1 mapping," *Magn. Reson. Med.* **64**, 1057–1067 (2010).

[12] Bjarnason, T. and Mitchell, J., "AnalyzeNNLS: Magnetic resonance multiexponential decay image analysis," *J. Magn. Reson.* **206**, 200–204 (2010).

[13] Whittall, K. and MacKay, A., "Quantitative interpretation of NMR relaxation data," *J. of Magn. Reson.* **84**(1), 134–152 (1989).

[14] Rice, S., "Mathematical analysis of random noise," *AT& T Tech. J.* **23**(3), 282–332 (1944).

[15] Gudbjartsson, H. and Patz, S., "The Rician distribution of noisy MRI data," *Magn. Reson. Med.* **34**(6), 910–914 (1995).

[16] den Dekker, A. J. and Sijbers, J., "Data distributions in magnetic resonance images: a review," *Phys. Medica* **30**(7), 725–741 (2014).

[17] van den Bos, A., *[Parameter Estimation for Scientists and Engineers]*. John Wiley & Sons, Inc., Hoboken, New Jersey (2007).

[18] Sijbers, J., den Dekker, A., Scheunders, P., and Van Dyck, D., "Maximum likelihood estimation of Rician distribution parameters," *IEEE T. Med. Imaging* **17**(3), 357–361 (1998).

[19] Sijbers, J., den Dekker, A. J., Raman, E., and Van Dyck, D., "Parameter estimation from magnitude MR images," *Int. J. Imag. Syst. Tech.* **10**(2), 109–114 (1999).

[20] O'Leary, D. and Rust, B., "Variable projection for nonlinear least squares problems," *Comput. Optim. Appl.* **54**(3), 579–593 (2012).

[21] Papoulis, A. and Pillai, S., *[Probability, Random Variables and Stochastic Processes with Errata Sheer]*. McGraw-Hill Education, New York, NY (2002).

[22] Poot, D., *Advances in the Reconstruction and Statistical Processing of Magnetic Resonance images*. PhD thesis, Universiteit Antwerpen (2010).

[23] Kay, S., *[Fundamentals of Statistical Signal Processing: Estimation Theory]*, ch. 1. Prentice Hall PTR, Upper Saddle River, NJ (1993).

[24] Norton, J., *[An Introduction to Identification]*, Dover Books on Electrical Engineering Series, Dover Publications (2009).

[25] van den Bos, A., *[Handbook of Measurement Science]*, vol. 1, ch. 8: Parameter Estimation, 331–377. Edited by P. H. Sydenham, Wiley, Chichester, England (1982).

[26] Lu, H., Nagae-Poetscher, L., and Golay, X., "Routine clinical brain MRI sequences for use at 3.0 Tesla," *J. Magn. Reson. Imag.* **22**, 13–22 (2005).

[27] Zhou, D. and Penn, R., "Full-brain T_1 mapping through inversion recovery fast spin echo imaging with time-efficient slice ordering," *Magn. Reson. Med.* **54**, 725–731 (2005).

[28] Wansapura, J., Holland, S., Dunn, R., and Ball, W., "NMR relaxation times in the human brain at 3.0 Tesla," *J. Magn. Reson. Imag.* **9**, 531–538 (1999).

[29] Gelman, N., Ewing, J., and Gorell, J., "Interregional variation of longitudinal relaxation rates in human brain at 3.0 T: Relation to estimated iron and water contents," *Magn. Reson. Med.* **45**, 71–79 (2001).

[30] Wright, P., Mougin, O., Totman, J., Peters, A., Brookes, M., Coxon, R., Morris, P., Clemence, M., Francis, S., Bowtell, R., and Gowland, P., "Water proton T_1 measurements in brain tissue at 7, 3 and 1.5T using IR-EPI, IR-TSE, and MPRAGE: Results and optimization," *Magn. Reson. Mater. Phy.* **21**, 121–130 (2008).

[31] Lin, C., Bernstein, M., Huston, J., and Fain, S., "Measurements of T_1 relaxation times at 3.0T: Implications for clinical MRA," *Proc. Int. Soc. Magn. Reson. Med.* (2001).

[32] Chatfield, C., *[Statistics for Technology: A Course in Applied Statistics, Third Edition]*, Chapman and Hall, London (1983).

[33] Stöcker, T. and Shah, N. J., "MP-SAGE: A new MP-RAGE sequence with enhanced SNR and CNR for brain imaging utilizing square-spiral phase encoding and variable flip angles," *Magn. Reson. Med.* **56**, 824–834 (2006).